DOI: 10.61782/fa.2023.1272

forum acusticum 2023

# SOC-BASED IMPLEMENTATION OF A MULTIPATH-RESILIENT BROADBAND UNDERWATER OFDM SYSTEM

**Jared Hermans** **George Sklivanitis*** **Dimitris A. Pados**

Center for Connected Autonomy and AI, Florida Atlantic University, Boca Raton, FL, USA

## ABSTRACT

Orthogonal Frequency Division Multiplexing (OFDM) is a multi-carrier modulation technique where a large number of closely spaced, in frequency, orthogonal sub-carriers are transmitted in parallel to form a single wide-band signal. With appropriate channel estimation and equalization at the receiver using known sub-carriers called pilots, the receiver can successfully correct for frequency selective fading – a common phenomenon in underwater acoustic channels. In this work, we will present the design and results from experimental evaluation of a high-rate OFDM transceiver that is implemented on a low-size, weight, power and cost System-on-Chip (SoC) based underwater acoustic modem. We carry out tests with broadband hydrophones with a usable frequency range up to 470 kHz in shallow water environments. The proposed transceiver enables link re-configurability with respect to bandwidth, number of pilot, null and data subcarriers, FFT size, and modulation and test link data rates up to 345 kbps in distances up to 9 m.

**Keywords:** *underwater IoT, system-on-chip, orthogonal frequency division multiplexing, broadband*

## 1. INTRODUCTION

The performance of underwater acoustic communication systems is measured through the bit error rate (BER) and the bandwidth efficiency, which have been subject of improvement for more than two decades of research work [1, 2]. Researchers have focused on different modulation techniques, starting from single carrier non-coherent modulation, coherent modulation, and nowadays, most of the scientific production is related with multi-carrier modulation techniques [1, 3–8].

Orthogonal Frequency Division Multiplexing (OFDM) is a type of multi-carrier modulation where a large number of closely spaced, in frequency, orthogonal sub-carriers, typically in a power of 2 to facilitate efficient implementation, are combined using an inverse Fast Fourier Transform (IFFT) and transmitted in parallel to form a single wide-band signal. There are many advantages offered by OFDM including high data rate, efficient spectrum utilization and robustness against frequency selective fading, or multipath. The orthogonality of the sub carriers ensures that they do not interfere with each other, even when spaced narrowly in frequency. In the frequency domain representation before the IFFT, the data sub-carriers contain a type of modulated symbol such as quadrature phase shift keying (QPSK) or quadrature amplitude modulation (QAM). In the time domain, after the IFFT, the OFDM signal is mixed onto a carrier and transmitted. At the receiver, an FFT is performed to convert the OFDM signal back to the frequency domain where the sub-carriers are demodulated.

In this paper, we present results from the development and evaluation of a highly-reconfigurable channel-aware OFDM transceiver on a low size, weight, power and cost (SWaP-C) System-on-Chip (SoC) based underwater acoustic modem [9]. We carry out tests with broadband hydrophones in both a laboratory tank (link distance of 1 m) and an outdoor pool (link distance of 9 m). We measure BER by manually reconfiguring link bandwidth, number of subcarriers and modulation order and demonstrate link data rates up to 345 kbps.

**Corresponding author*: gsklivanitis@fau.edu.

## 2. MODEM ARCHITECTURE

The low-size, weight, power and cost underwater acoustic (UW-A) modem is built around a custom PCB developed in-house at the Center for Connected Autonomy and AI at Florida Atlantic University as shown in [9]. On the transmit side, the modem receives analog baseband data from a Xilinx ZYNQ XC7Z010 System-on-Chip (SoC) [10] that is interfaced with a 14-bit 10 MSPS digital-to-analog-converter (DAC) and feeds them to a power amplifier. The resulting signals are fed through a transmit/receive switch to a Teledyne RESON TC-4013 or TC-4034 miniature wideband hydrophone that is used both for projecting and receiving sound in a time division fashion. The receive side is symmetrical, with a pre-amplifier, a variable gain amplifier and a 14-bit 40 MSPS analog-to-digital (ADC) converter, which are then fed into the Xilinx ZYNQ SoC. The operating frequency range of the TC-4013 is 1 Hz to 170 kHz and 1 Hz to 480 kHz for the TC-4034. The modem can support either broadband or narrowband transducers. These transducers were selected mainly because of the relatively wide frequency bands that they can support, which allow high data rate communications and enable the implementation of a variety of physical layer schemes. TC-4013s provide receiving sensitivity of $-211$ [dB re 1V/µPa at 1 m] that is relatively flat over the operational frequency range and transmitting sensitivity of 130 [dB re 1µPa/V at 1 m] at 100 kHz. TC-4034 provide receiving sensitivity of $-218$ [dB re 1V/µPa at 1 m] at 250 Hz and transmitting sensitivity of 122 [dB re 1V/µPa at 1 m] at 100 kHz. Both transducers have omnidirectional horizontal and 270° vertical directivity patterns at 100 kHz (for TC-4013) and 300 kHz (for TC-4034), respectively.

## 3. OFDM SYSTEM DESIGN

### 3.1 Reconfiguration Parameters

The proposed underwater acoustic (UW-A) OFDM system shown in Fig. 1 is designed to be as parameterized as possible to support a wide range of environments, hydrophones and throughput and resiliency requirements. Parameters such as the total number of subcarriers $K$, the FFT size $N_{FFT}$, bandwidth $B$, null sub-carrier $K_N$ size, pilot sub-subcarriers $K_P$ size, cyclic prefix length (CP), modulation order $M$, OFDM symbol guard period $T_g$, synchronization symbol root index and OFDM symbols-per-frame are all user-configurable to tailor the system to the environment and application requirements. As $K$ increases for a given bandwidth $B$, both the bandwidth efficiency and the coherence between adjacent carrier increase, this causes the carrier spacing $\Delta f = \frac{B}{K}$ to become smaller. Parameters have the capability of configurability on a per frame basis with the exception of bandwidth which requires partial reconfiguration of the programmable logic (PL) due to the FIR filter implementation [11].

### 3.2 Sub-Carrier Allocation and Resource Management

Sub-carrier allocation is an important part of designing an OFDM system to maximize spectral efficiency, optimize resource allocation, mitigate multipath and other forms of interference and ensure requirements for throughput and multi-user support [1, 3]. Sub-carriers are allocated as either data, pilot or null sub-carriers. Pilot sub-carriers carry known information which the receiver uses for channel estimation and equalization. Null sub-carriers are zeroed out sub-carriers typically placed at the edges of the bandwidth and at DC to prevent distortion or attenuation introduced by the digital upconverter/downconverter (DUC/DDC) and to prevent a DC offset at the transmitter or receiver.

### 3.3 Cyclic Prefix

In OFDM, the cyclic prefix (CP) is the ending fractional portion of the time domain OFDM symbol appended to the beginning of the OFDM symbol. At the expense of data rate and transmitted power, there are several desirable characteristics of CP [12]:

- Guard interval: The added CP samples between adjacent symbols provide a buffer period in the time domain.
- Synchronization and frequency domain equalization: Synchronization is not perfect under channel conditions and can be off several samples to several hundred samples. With CP, timing offset (in time domain) is expressed as phase offset in frequency domain which is easily corrected by a frequency domain equalizer due to circular convolution properties of CP.
- ISI rejection: Since CP is a copy of the useful symbol, any interference affecting the CP will be eliminated during the receiver's processing.

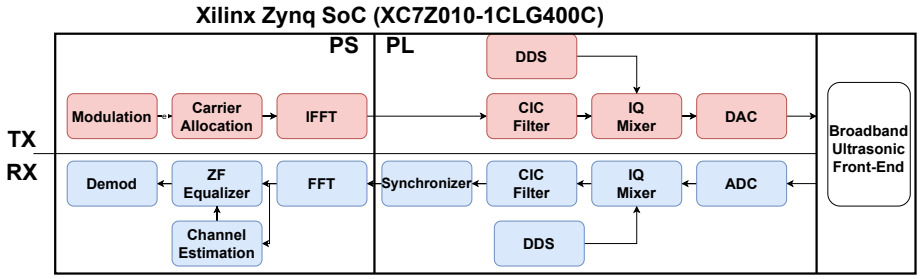


**Figure 1**. Proposed UW-A OFDM system.

### 3.4 Digital Up- and Downconversion

These conversions sit between the ADC and digital baseband stages, and comprise a frequency translation of the signal (between baseband and the modulated carrier frequency, and vice versa), and a change in sampling rate.

DDC forms part of the receiver, and is the first processing stage following the ADC. The architecture of the DDC is presented in Figure 2. The DDC first shifts the incoming modulated signal from a carrier frequency to baseband, by mixing it with the output of a Numerically Controlled Oscillator (NCO).

The Digital Upconverter (DUC), which is part of the transmitter, performs a similar but mirrored set of operations to the DDC. First, the low sampling rate of the digital baseband stage, $f_s$, is increased to the much higher rate used by the DAC (10 MSPS), by an interpolator. The interpolated signal is then modulated by mixing it with sine and cosine signals generated by an NCO, at the desired carrier frequency, $f_c$.

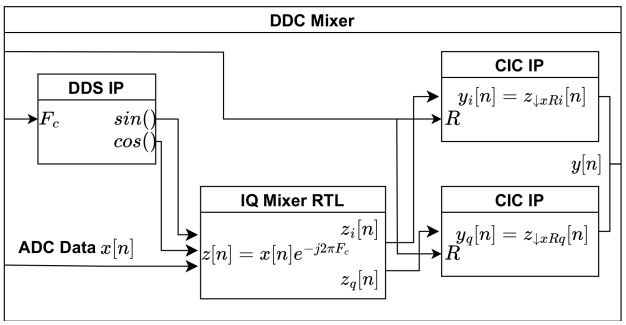


**Figure 2**. Resource-efficient DDC design.

Utilizing a cascaded integer comb (CIC) filter IP core [13] and a custom IQ mixer, a low resource DUC and DDC mixer are implemented. The CIC filter is a type of FIR filter primarily used for interpolation and decimation with efficient implementation [13]. The transfer function for the CIC filter is expressed in terms of decimation or interpolation factor and the number of stages:

$$H(z) = \frac{(1 - z^{-1})^N}{1 - z^{-R^{N-1}}} \tag{1}$$

where $R$ is the decimation or interpolation factor and $N$ is the number of stages. One drawback of the CIC filter is the frequency response as seen in Fig. 3 when compared to a 512-tap complex FIR filter. Both filters correspond to a 40x interpolation factor and a cutoff frequency of $\pi/R = 0.025\pi$ rad/sample, however the CIC filter has a much larger transition bandwidth and larger ripples. This will cause the OFDM spectrum towards the edges of the nyquist zone to be attenuated, and distortion - although small - will be introduced. As mentioned earlier, setting a number of null sub-carriers at the edges of the nyquist zone will avoid attenuation of data sub-carriers.

IQ mixing up-converts the complex baseband OFDM signal up to a real, passband signal at the carrier frequency. This is implemented with a programmable direct digital synthesis (DDS) IP core (which generates sine and cosine) and a complex multiplier adder:

$$\Phi(n) = I(n)\cos(2\pi f_c n) - Q(n)\sin(2\pi f_c n). \tag{2}$$

### 3.5 Frame Synchronization

OFDM frame synchronization is the process of achieving accurate timing between transmitter and receiver. This is achieved with correlation at the receiver with a known Zadoff-Chu sequence transmitted as the first OFDM symbol - called a synchronization symbol [14]. The Zadoff-Chu (ZC) sequence is selected for the synchronization symbol due to desirable autocorrelation and cross-correlation properties. Also, the ZC sequence has a

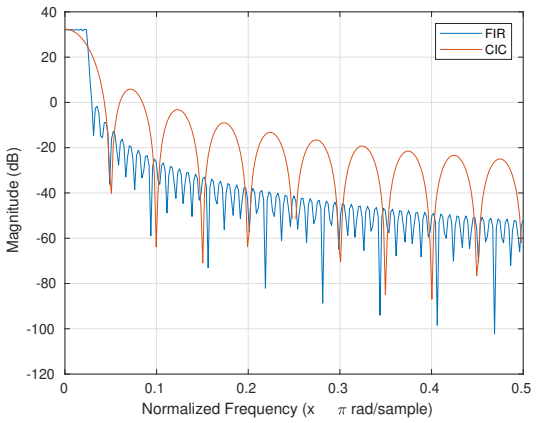


**Figure 3**. Frequency response of 512-tap complex FIR filter vs two-stage CIC filter.

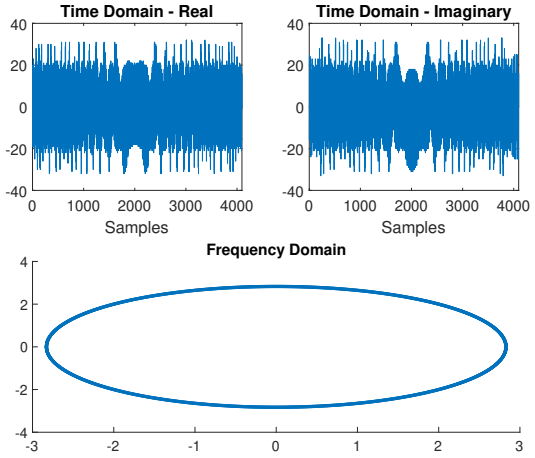


**Figure 4**. Zadoff-Chu synchronization symbol.

low peak to average power ratio (PAPR) which allows it to be transmitted at a higher average power than the data OFDM symbols resulting in more accurate synchronization in low SNR channels. The ZC sequence is given by:

$$Z(n) = \exp\left(-j\pi u \frac{n(n+1)}{N}\right) \tag{3}$$

where $u$ is the ZC root index and $N$ is the length of the ZC sequence. We choose $u = 13$ and $N = 2053$ and truncate the length to 2048 [14]. Taking the 4096 point IFFT of the sequence such that the signal occupies 50% of the BW, the time domain samples shown in Fig. 4. For the match filter in the receiver, the reverse conjugate of the time domain samples is used as taps in the in-phase (I) and quadrature (Q) 4096 tap reconfigurable FIR filters. Once the full synchronization symbol passes through the match fiter, there will be a single large peak at the filter output, as shown in Fig. 5, in which the receiver synchronizes to.

### 3.6 Channel Estimation and Equalization

Equalization is a technique used in digital communications to mitigate the effects of channel distortion and intersymbol interference (ISI) at the receiver and recover the transmitted symbols. The proposed system utilizes a zero-forcing (ZF) equalizer which works by estimating the channel response using pilot sub-carriers at known locations in frequency and applying the inverse of that response to the data symbols. Channel estimation occurs in the frequency domain:

$$\hat{H}[k] = \frac{P_r[k]}{P_t[k]}, \quad k = 1, \ldots, K_P \tag{4}$$

where $k$ is the sub-carrier index at pilot locations, $P_r[k]$ is the $k$-th received pilot sub-carrier and $P_t[k]$ is the $k$-th transmitted pilot sub-carrier. Pilot selection for the ZF channel estimation is chosen to be the same modulation order as the data sub-carriers as they provide a more accurate representation of the channel characteristics. Drawbacks of ZF channel estimation is that in the presence of noise or interference (other than ISI), errors are introduced into the channel estimation [15] and if nulls exist in the frequency response, noise is increased at the location of the null [16]. We can reduce errors introduced into the channel estimation from noise with averaging techniques. However, due to the large frequency selective fading of underwater acoustic channels, this method is not employed by the proposed system. Instead, with the channel estimation at pilot locations, the channel estimate is then interpolated to include all sub-carriers $K$ and used to equalize the data sub-carriers $K - K_N - K_P$:

$$Y[k] = \frac{X[k]}{\hat{H}^*[k]}, \quad k = 1, \ldots, K - K_N - K_P \tag{5}$$

where $X[k]$ is the received data sub-carrier and $\hat{H}[k]$ is the channel estimate acquired by (4).

## 4. PERFORMANCE EVALUATION

We characterize the OFDM system performance first with the TC-4013 hydrophone then with the higher bandwith TC-4034 hydrophone. Bit error rate (BER) measurements – without error correction – were determined over the transmission of a single 16 OFDM symbol (without accounting for the synchronization sequence) OFDM frame. Initial field testing started in a $1.5\,\mathrm{m} \times 2.4\,\mathrm{m} \times 0.9\,\mathrm{m}$ laboratory water tank shown in Fig. 9 and moved to a $7.6\,\mathrm{m} \times 9.1\,\mathrm{m} \times 4.6\,\mathrm{m}$ pool.

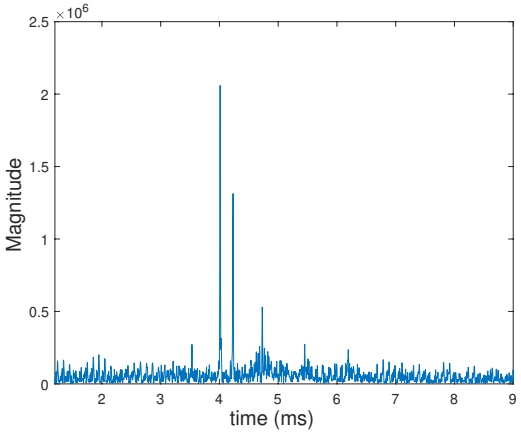


**Figure 5**. Channel sounding with OFDM frame synchronization symbol with TC-4034 in the tank.

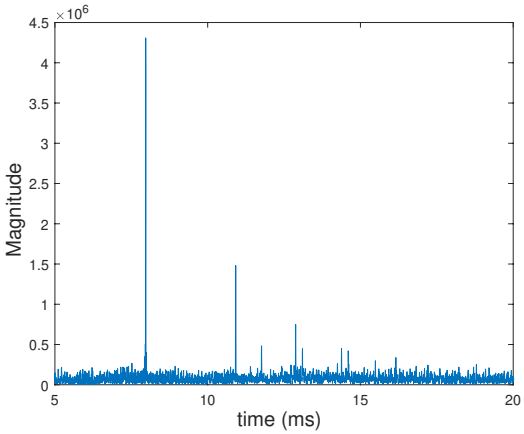


**Figure 6**. Channel sounding with OFDM frame synchronization symbol with TC-4034 in the pool.

Time domain and frequency domain samples after the DDC are saved in a parallel thread and later plotted in MATLAB. The synchronizer's matched filtered output samples are captured with an integrated logic analyzer (ILA) programmed on the PL.

Using the TC-4013 with a usable frequency range of 1 Hz to 170 kHz, an OFDM carrier is configured with a $\mathrm{f_c} = 125\,\mathrm{kHz}$, $\mathrm{B} = 50\,\mathrm{kHz}$, null sub-carrier density of 30%, i.e., $K_N = 1229$ (effective bandwidth of 35 kHz), pilot sub-carrier density of 50% i.e., $K_P = (N_{FFT} - K_N) * 50\% = 1434$, BPSK modulation, $K = N_{FFT} = 4096$, $CP = 256$, $\mathrm{T_g} = 1\,\mathrm{ms}$ guard period obtains a symbol data rate of $16.464\,\mathrm{kbps}$ and a frame data rate of $16.28\,\mathrm{kbps}$ using the following:

$$bps = \frac{\log_2 M}{T}(N_{FFT} - K_N - K_P) \tag{6}$$

where $T = \frac{N_{FFT}+CP}{B}$ for symbol data rate and $T = \frac{N_{FFT}+CP}{B} + T_g$ for frame data rate. BER was determined to be $0.007639$. Increasing the modulation order to $M = 4$ and in turn increasing symbol throughput to $32.927\,\mathrm{kbps}$ and frame throughput to $32.55\,\mathrm{kbps}$, BER was determined to be $0.02507$. The received spectrum and constellation is visibly affected by frequency selective fading from both the hydrophone frequency response and the underwater frequency response as seen in Fig. 10. Although the spectrum is greatly distorted, at the output of the ZF equalizer we can still see the QPSK constellation in Fig. 11

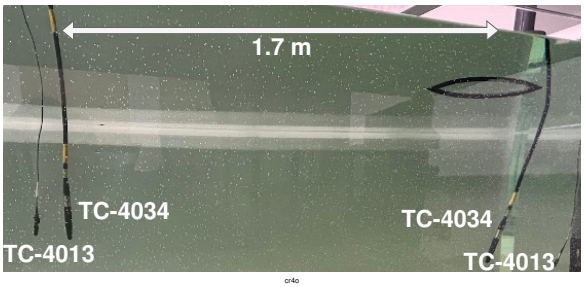


**Figure 7**. Laboratory tank setup with TC-4013 and TC-4034 transmit and receive hydrophones.

Moving to the TC-4034 which supports larger bandwidths and higher frequencies we configure an OFDM carrier with a $\mathrm{f_c} = 290\,\mathrm{kHz}$, $\mathrm{B} = 250\,\mathrm{kHz}$, $K_N = 1229$ (effective bandwidth of $175\,\mathrm{kHz}$), $K_P = 1434$, BPSK modulation, $K = N_{FFT} = 4096$, $CP = 256$ and $\mathrm{T_g} = 1\,\mathrm{ms}$ guard period obtains a symbol data rate of

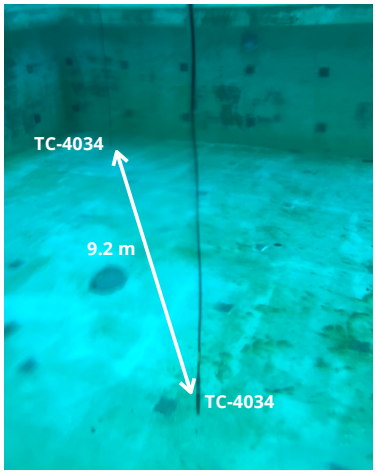


**Figure 8**. Pool setup with TC-4034 transmit and receive hydrophones.

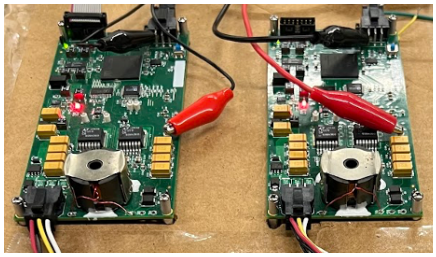

**Figure 9**. Low SWaP-C modems [9] interfaced with TC-4013 and TC-4034 hydrophones.

82.3 kbps. BER was determined to be 0.01875 in the tank and 0.009066 in the pool (with increasing $T_g = 10$ ms decreasing packet data rate from 77.85 kbps to 52.28 kbps with same symbol data rate). Looking at Fig. 12 and Fig. 13 large amounts of frequency selective fading is also present just as the TC-4013.

With ILA capture at the matched filter output of the synchronizer in Fig. 5 and Fig. 6 we see multiple peaks which indicate the line of sight as well as several reverberations. In the tank, the first echo arrives with a delay of 55 samples or 0.22 ms and the second echo arrives with a delay of 124 samples or 0.496 ms. The delay spread falls within the 256 sample CP and the 1 ms guard period. In the pool, where range has increased by about 7x, there are visible reverberations at 2.944, 3.792, 4.9, 5.132, 6.4, 6.63 and 8.2 ms. The delay spread falls within the increased $T_g = 10$ ms guard period.

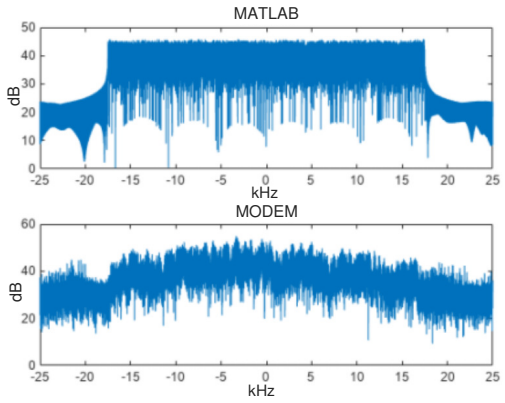


**Figure 10**. Ideal vs underwater channel FFT input spectrum with TC-4013, $f_c = 125$ kHz, effective bandwidth of 35 kHz in the tank.

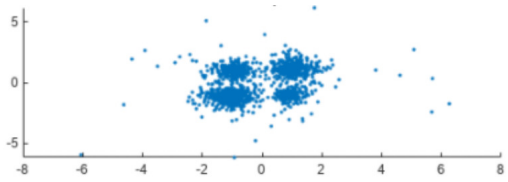

**Figure 11**. Received constellation with $K = N_{FFT} = 4096$ OFDM with TC-4013 in the tank.

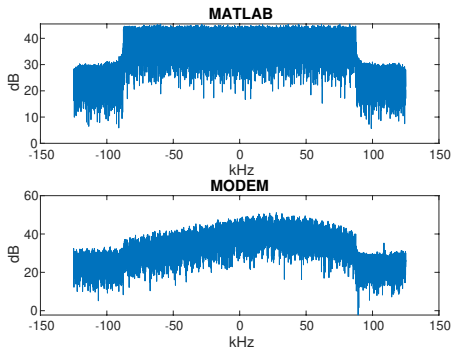


**Figure 12**. Ideal vs underwater channel FFT input spectrum with TC-4034, $f_c = 290$ kHz, effective bandwidth of 175 kHz in the tank.

When increasing the $N_{FFT}$ size, error vector magnitude (EVM) observably dropped allowing for an in-

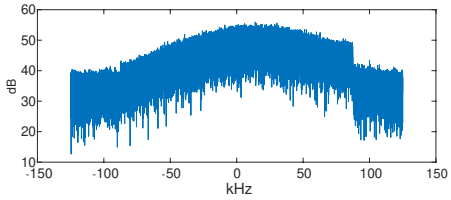


**Figure 13**. FFT input spectrum with TC-4034, $f_c = 290$ kHz, effective bandwidth of 175 kHz in the pool.

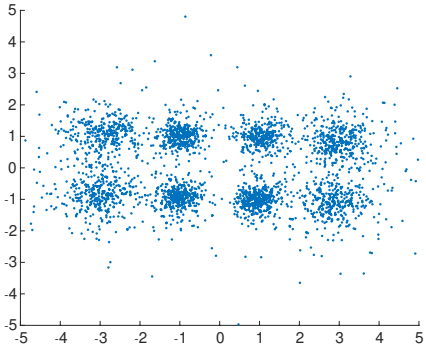

**Figure 14**. Received constellation with $K = N_{FFT} = 8192$ OFDM with TC-4034 in the tank.

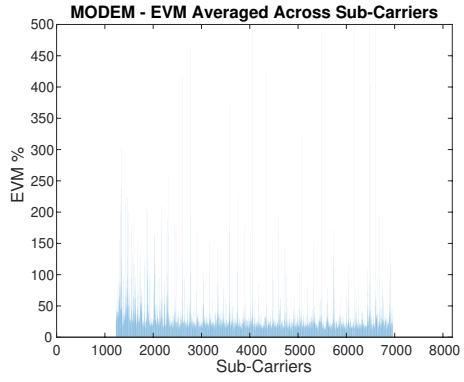


**Figure 15**. Error vector magnitude of $K = N_{FFT} = 8192$ OFDM with TC-4034 in the tank.

crease in modulation order. Increasing to $N_{FFT} = 8192$ and modulation order $M = 8$ from the previous test yielded a symbol data rate of 254 kbps, a frame data rate of 247.2 kbps and a BER of 0.0186 in the tank.

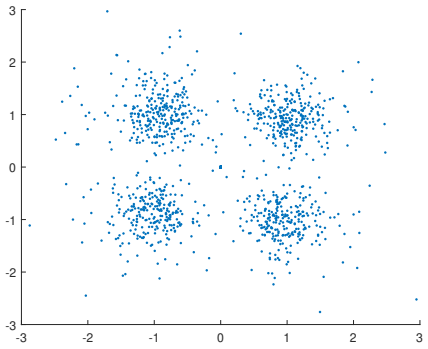

**Figure 16**. Received constellation with $K = N_{FFT} = 8192$ OFDM with TC-4034 in the pool.

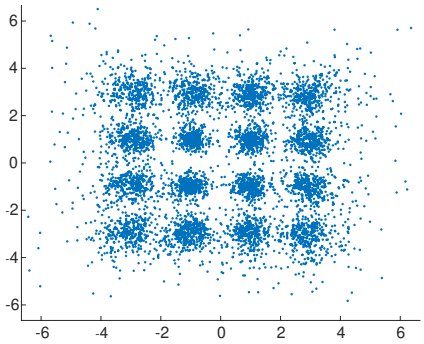

**Figure 17**. Received constellation with $K = N_{FFT} = 16384$ OFDM with TC-4034 in the tank.

EVM vs. data sub-carriers averaged across an OFDM frame is shown in Fig. 15. For the pool test, BER was higher than 0.05 so the modulation order was lowered to QPSK, shown in Fig. 16, dropping symbol throughput to 170 kbps and packet throughput to 131 kbps which resulted in a BER of 0.03408.

The final test increases $N_{FFT} = 16384$ and $M = 16$ from the previous test resulting in a 345 kbps symbol data rate, a 339.5 kbps frame data rate and a BER of 0.018 in the tank. The equalized constellation is shown in Fig. 17. Noise and fading was too high to go above QPSK modulation in the pool test.

## 5. CONCLUSIONS

We demonstrated through extensive underwater tests that the proposed low SWaP-C underwater acoustic modem can achieve up to 345 kbps in distances up to 9 m. The proposed implementation of a highly-reconfigurable OFDM transceiver supports multiple broadband hydrophones. Future work will focus on autonomous reconfiguration of OFDM parameters such as number of subcarriers, modulation and bandwidth for robust operation in multipath underwater environments.

## 6. ACKNOWLEDGEMENTS

This work is supported in part by the National Science Foundation under Grant No. CNS 1753406, the Schmidt Family Foundation, and a seed funding award from the FAU College of Engineering and Computer Science and the FAU Institute for Sensing and Embedded Networks Systems Engineering.

## 7. REFERENCES

[1] S. Zhou and Z.-H. Wang, *OFDM for Underwater Acoustic Communications*. John Wiley and Sons, Inc., 2014.

[2] T. Melodia, H. Kulhandjian, L.-C. Kuo, and E. Demirors, *Advances in Underwater Acoustic Networking*, ch. 23, pp. 804–852. John Wiley Sons, Ltd, 2013.

[3] A. Radosevic, R. Ahmed, T. Duman, J. Proakis, and M. Stojanovic, "Adaptive OFDM modulation for underwater acoustic communications: Design considerations and experimental results," *IEEE Journal of Oceanic Engineering*, vol. 39, pp. 357–370, April 2014.

[4] E. Demirors, G. Sklivanitis, G. E. Santagati, T. Melodia, and S. N. Batalama, "A high-rate software-defined underwater acoustic modem with real-time adaptation capabilities," *IEEE Access*, vol. 6, pp. 18602–18615, 2018.

[5] E. Demirors, G. Sklivanitis, T. Melodia, S. N. Batalama, and D. A. Pados, "Software-defined underwater acoustic networks: toward a high-rate real-time reconfigurable modem," *IEEE Communications Magazine*, vol. 53, no. 11, pp. 64–71, 2015.

[6] G. Sklivanitis, E. Demirors, S. N. Batalama, T. Melodia, and D. A. Pados, "Receiver configuration and testbed development for underwater cognitive channelization," in *2014 48th Asilomar Conference on Signals, Systems and Computers*, pp. 1594–1598, 2014.

[7] A. Bourré, S. Lmai, C. Laot, and S. Houcke, "A robust OFDM modem for underwater acoustic communications," in *2013 MTS/IEEE OCEANS - Bergen*, pp. 1–5, 2013.

[8] S. Mangione, G. E. Galioto, D. Croce, I. Tinnirello, and C. Petrioli, "A channel-aware adaptive modem for underwater acoustic communications," *IEEE Access*, vol. 9, pp. 76340–76353, 2021.

[9] J. Hermans, G. Sklivanitis, and D. A. Pados, "A first-of-its-kind low size, weight and power run-time reconfigurable underwater modem," in *2022 Sixth Underwater Communications and Networking Conference (UComms)*, pp. 1–5, IEEE, 2022.

[10] Xilinx, "Zynq-7000 All programmable SoC technical reference manual (ug585)," tech. rep., Tech. rep., Xilinx, 2014, https://www. xilinx. com/support/documentation, 2014.

[11] LogiCORE, "FIR Compiler v5.0, Xilinx," *Inc., San Jose, CA, USA*, 2010.

[12] S. Chen and C. Zhu, "ICI and ISI analysis and mitigation for ofdm systems with insufficient cyclic prefix in time-varying channels," *IEEE Transactions on Consumer Electronics*, vol. 50, no. 1, pp. 78–83, 2004.

[13] V. Elamaran, R. Vaishnavi, A. M. Rozario, S. M. Joseph, and A. Cherian, "CIC for decimation and interpolation using xilinx system generator," in *2013 International Conference on Communication and Signal Processing*, pp. 622–626, IEEE, 2013.

[14] J. G. Andrews, "A primer on zadoff chu sequences," *arXiv preprint arXiv:2211.05702*, 2022.

[15] A. Trimeche, N. Boukid, A. Sakly, and A. Mtibaa, "Performance analysis of ZF and MMSE equalizers for mimo systems," in *7th International Conference on Design & Technology of Integrated Systems in Nanoscale Era*, pp. 1–6, IEEE, 2012.

[16] P. Sharma, "Performance analysis of zero-forcing equalizer for ISI reduction in wireless channels," *International Journal of Engineering Research & Technology*, vol. 1, no. 8, pp. 1–7, 2012.